

# Flavor-dependent EMC effect from a nucleon swelling model

Rong Wang<sup>1,\*</sup>, Raphaël Dupré<sup>1</sup>, Yin Huang<sup>2</sup>, Baiyang Zhang<sup>3</sup>, and Silvia Niccolai<sup>1</sup>

<sup>1</sup> *Institut de Physique Nucléaire, CNRS-IN2P3, Univ. Paris-Sud,  
Université Paris-Saclay, 91406 Orsay Cedex, France*

<sup>2</sup> *School of Physics and Nuclear Energy Engineering,  
International Research Center for Nuclei and Particles in the Cosmos  
and Beijing Key Laboratory of Advanced Nuclear Materials and Physics,  
Beihang University, Beijing 100191, China and*

<sup>3</sup> *Wigner Research Center for Physics, H-1121 Budapest, Hungary*

(Dated: March 1, 2022)

We present our results for a flavor-dependent EMC effect based on the nIMParton nuclear PDFs, in which the  $x$ -dependence is described with a nucleon swelling model. The nuclear correction from nucleon swelling is considered through a modification of the initial valence quark distributions instead of a dynamical rescaling. To probe the flavor-dependence of the model, the experimental observables are calculated applying nIMParton nuclear modifications for various experiments: parity-violating deep inelastic scattering on nuclear target, pion-induced Drell-Yan, and W-boson production in proton-nucleus collisions. In addition, we present the expected effect for the spectator-tagged deep inelastic scattering process, which will be performed by the CLAS12 collaboration with the ALERT detector.

## I. INTRODUCTION

Since the discovery of the EMC effect [1], both particle and nuclear physics communities have struggled to understand the impact of the nuclear medium and of the binding of nucleons on the nucleon structure. The intricate connection between the perturbative and nonperturbative mechanisms involved in these questions are typical of the underlying Quantum Chromodynamics (QCD) theory. Nonetheless, numerous models have been proposed to understand the EMC effect in the past decades (see the following reviews [2–7]). Generally, many models describe fairly well the main features of the EMC effect. Therefore, new data about the EMC effect is crucial to constrain the models and to understand the EMC effect.

Up to now, the  $x$ ,  $Q^2$ , and  $A$  dependence of the EMC ratios have been investigated with a large number of experimental measurements. Basically all the models depict well the  $x$ -dependence of the EMC ratios. The  $Q^2$ -dependence of structure function ratio is found to be weak in experiments, and the  $Q^2$ -dependence of nuclear parton distribution functions (PDFs) obeys the QCD-based DGLAP evolution which governs the  $Q^2$ -dependence of free nucleon PDFs as well [8–10]. The recent measurement of the nuclear dependence of the EMC effect at JLab [11] implies that the EMC effect dominantly originates from the high virtuality or the high local density [5, 6, 12, 13]. The detailed study of the flavor-dependence of the EMC effect is one of the next directions for future experiments [7, 14–16]. Investigating the variations of the nuclear medium modifications for quarks of different flavors opens a new window to test the various models.

The CBT model [14, 17–19] is the first model to bring out the nuclear effect difference between up quark and down quark. In CBT model, the nuclear PDFs are determined using a confining Nambu-Jona-Lasinio model, where the nucleon is approximated as a quark-diquark bound state in the Faddeev equation [17]. The nuclear effect is implemented with the scalar and vector mean fields coupling to the quarks, and the strength of the mean fields are self-consistently determined using an equation of state for nuclear matter. The isovector-vector mean field  $\rho^0$  arisen from neutron or proton excess in nuclei breaks down  $u_p(x) = d_n(x)$  and  $d_p(x) = u_n(x)$  for bound nucleons, resulting in the flavor-dependence of the EMC effect.

Recently, nIMParton (nuclear “I’M Parton”) global analysis studied the nuclear parton distributions with a nonperturbative input which consists of only three valence quarks [20, 21]. Instead of adding degrees of freedom from nuclear physics, the EMC effect in nIMParton analysis is produced from the deformation of valence quark distributions at the input scale  $Q_0^2$  due to the mechanism of nucleon swelling. The influence of the nuclear interactions or the mean-field mesons are all reflected in the “swelled” nucleon in the model. According to the Heisenberg uncertainty principle, the larger confinement size gives rise to smaller widths of the momentum distributions of partons. The nuclear PDFs at high  $Q^2$  are then dynamically generated from the QCD-based evolution [20] with the modified valence quark distributions. The nIMParton nuclear modification factors for up, down and strange quarks present some differences. There are no initial strange quarks at the input scale  $Q_0^2$ . All the strange quarks are generated from gluon splitting in QCD evolution. This is why the nuclear medium modification of strange quark distribution is different from that of valence quarks. The nuclear modifications of up and down quarks manifest some difference, and it is due to

\* wangrong@ipno.in2p3.fr

the width difference between the up valence quark distribution and the down valence quark distribution. Inside the proton, the width of down valence quark distribution is narrower than that of up valence quark distribution. With the same size of confinement increase, the down valence quark distribution deforms more greatly to meet the condition of Heisenberg uncertainty principle.

On the experimental side, several high energy scattering processes are suggested to observe the flavor-dependence of the EMC effect [14–16]. They are the parity-violating deep inelastic scattering (PVDIS) process with a polarized electron beam [14], the pion-induced Drell-Yan (DY) processes with pion beams [15], and the W-boson production with high energy proton-nucleus collisions [16]. In these experiments, the sensitivities to the flavor-dependence of the EMC effect are all discussed under the CBT model. It is worthwhile and important to see also the predictions from other models. In this paper, we show the predicted experimental observables of above experiments using the flavor-dependent nuclear effect from nIMParton nuclear PDFs. Although the flavor-dependence of nIMParton model is weak, it provides a baseline to understand the nuclear isovector force in CBT model.

Another, recently proposed, method to access the flavor dependent structure functions is to detect the low energy recoil nuclei. A program of such measurements using A Low Energy Recoil Tracker (ALERT) combined with the CLAS12 detectors has been approved at JLab [22–24]. With the spectator tagged, one knows the type of the nucleon struck by the high energy probe. The EMC effect of the bound proton and the bound neutron can then be independently measured, which could shed some lights on the isospin-dependence of the EMC effect. In this work, we also give predictions for the EMC effect difference between the nuclear medium modified proton and the nuclear medium modified neutron.

In Sec. II, we review the nucleon swelling model used to explain the EMC effect. The size of nucleon swelling obtained from nIMParton analysis is compared with the experimental measurements and the model calculations. The nIMParton analysis based on the nucleon swelling and the flavor-dependence of the nuclear effect are introduced in Sec. III. The experimental observables of PVDIS process, pion-induced DY process and p-A collisions are shown in Sec. IV, Sec. V and Sec. VI respectively, applying nIMParton nuclear PDFs. In Sec. VII, we discuss the potential of tagged-DIS to probe the flavor-dependence of the EMC effect. Lastly, a brief summary is given in Sec. VIII.

## II. NUCLEON SWELLING AND THE EMC EFFECT

The models of the EMC effect can be roughly classified in two categories: conventional nuclear physics models and the QCD-inspired models [2]. The conventional

nuclear models usually take into account the reduced nucleon mass in medium or the virtuality, which gives the  $x$ -rescaling models [25–30] ( $x = Q^2/(2m_N\nu)$ ) and the off-shellness corrections [31–35]. The QCD-inspired models usually require an increase of the quark confinement, or a simple increase of nucleon radius (nucleon swelling). A bigger nucleon equals a higher resolution power of the probe. In the language of QCD evolution, the  $Q^2$ -rescaling [36–40] (an higher resolution power) is carried out to interpret the effect.

The nucleon swelling discussed in this work refers to the increase of the quark confinement size. Such quark confinement enlargement is present in the multi-quark cluster models [41–45], while a smaller quark deconfinement is predicted in the Quark-Meson Coupling (QMC) model [46–48], and the nuclear potential model [54–56]. In the multi-quark cluster model, the heavy nuclei favor the formations of large multi-nucleon clusters containing  $3N$  ( $N = 1, 2, 3, \dots$ ) valence quarks. In the QMC model, the size of the non-overlapping nucleon bag changes with the exchange of the mean-field meson. In the potential model, the three-quark quantum system are modified by the nuclear attractive potential.

There are a few experiments which indicated an increase of the quark confinement radius in the nuclear medium [49–52]. The nucleon swelling is found to be small for the Helium-3 nucleus through a quasi-elastic scattering experiment, which is smaller than 3-6 percentage [49]. The other experiment, with kaon probe, hints to an increase of the confinement up to 20% in  $^{12}\text{C}$  and  $^{40}\text{Ca}$  [50]. Furthermore, an interesting analysis of the data of hadron-nucleus interaction shows that the effective cross section with bound nucleon is slightly larger than that with free nucleon, which could imply a size increase as well [53].

In nIMParton, the increase of the nucleon size is obtained from a global analysis to the nuclear DIS data from worldwide facilities. To reproduce the data, we find swellings of the nucleon radius of 0.8%, 2% and 8% for deuteron,  $^3\text{He}$  and  $^{208}\text{Pb}$  respectively [20]. The size of the estimated nucleon swelling from experiments and from various models are listed in Table I. We see that several models predict such effects of a few percent, such as the QMC model [48], the binding potential model [54], the Skyrmion model [55], the quark-nucleon interaction model [56], the chiral quark-soliton model [57], the chiral symmetry restoration model [58], the weak stretching model [59], the PLC-suppression model [60], and the statistical model [61].

Regardless of the origin of nucleon swelling, the valence quark distributions are redistributed according to uncertainty principle to adapt for a larger spacial uncertainty [20]. In our model, all the medium modifications are reflected by this simple picture of an increase of quark confinement, which changes the widths of momentum distributions [20]. The definition of the widths of valence

TABLE I. The magnitudes of nucleon swelling inferred from experiments and predicted from various models.

experiment/model	size of nucleon swelling
quasielastic scattering [49]	< 3 – 6% for $^3\text{He}$
$K^+$ -nucleus scattering [50]	10 – 30% for $^{12}\text{C}$ and $^{40}\text{Ca}$
nIMParton [20]	2.0 – 8.1% for $^3\text{He}$ - $^{208}\text{Pb}$
QMC [48]	5.5% for typical nuclei
binding potential [54]	a few % for typical nuclei
Skyrmion model [55]	3 – 4%
quark-N interaction [56]	$\sim 2\%$ for nuclear matter
chiral quark-soliton [57]	$\sim 2.4\%$ for heavy nuclei
chiral symmetry [58]	< 10% for nuclear matter
N-N overlapping [37]	4.7 – 22% for $^3\text{He}$ - $^{208}\text{Pb}$
weak stretching [59]	4.5 – 9.4% for $^4\text{He}$ - $^{208}\text{Pb}$
PLC-suppression [60]	1 – 3%
statistical model [61]	2.2 – 5.0% for $^4\text{He}$ - $^{197}\text{Au}$
quark-quark correlation [62]	15%
chiral quark-meson [63]	$\sim 19\%$ for nuclear matter
string model [64]	40%

distributions are written as,

$$\begin{aligned}
 \sigma(x_u) &= \sqrt{\langle x_u^2 \rangle - \langle x_u \rangle^2}, \\
 \sigma(x_d) &= \sqrt{\langle x_d^2 \rangle - \langle x_d \rangle^2}, \\
 \langle x_u \rangle &= \int_0^1 x \frac{u_v(x, Q_0^2)}{2} dx, \\
 \langle x_d \rangle &= \int_0^1 x d_v(x, Q_0^2) dx, \\
 \langle x_u^2 \rangle &= \int_0^1 x^2 \frac{u_v(x, Q_0^2)}{2} dx, \\
 \langle x_d^2 \rangle &= \int_0^1 x^2 d_v(x, Q_0^2) dx,
 \end{aligned} \tag{1}$$

and the deformation of the width of nuclear valence distribution is modeled with a in-medium nucleon swelling parameter  $\delta_A$ . The momentum width is inversely proportional to the nucleon size, as shown in the following equation,

$$\frac{\sigma(x_q^A)}{\sigma(x_q^N)} = \frac{R_N}{R_{\text{in-medium } N}} = \frac{1}{1 + \delta_A}, (q = u, d). \tag{2}$$

For simplicity and because we lack information on the question, the swellings of the bound proton and the bound neutron are identical in the model, moreover the up and down valence quarks are confined in the same enlarged space. In these conditions, the flavor-dependence of the EMC effect comes from the difference in widths of the initial up and down valence quark distributions. In consequence, when the confinement radius changes, the PDF ratio of down valence quark is more affected than the ratio of up valence quark. This effect is mainly affecting the range of  $0.1 < x < 0.5$  at high  $Q^2$  [20].

Fig. 1 shows the nuclear modifications on the initial valence quark distributions for  $^{40}\text{Ca}$ . The EMC effect is the result by adjusting the widths of nuclear quark distributions. Since the width of down valence quark distribution is narrower, the width of  $d^{\text{p in Ca}}/d^{\text{p}}$  curve is also narrower. In the calculation, the valence quark distributions of both the free proton and the bound proton are parameterized as  $Ax^B(1-x)^C$ , and they are required to satisfy the momentum sum rule and the valence sum rule.

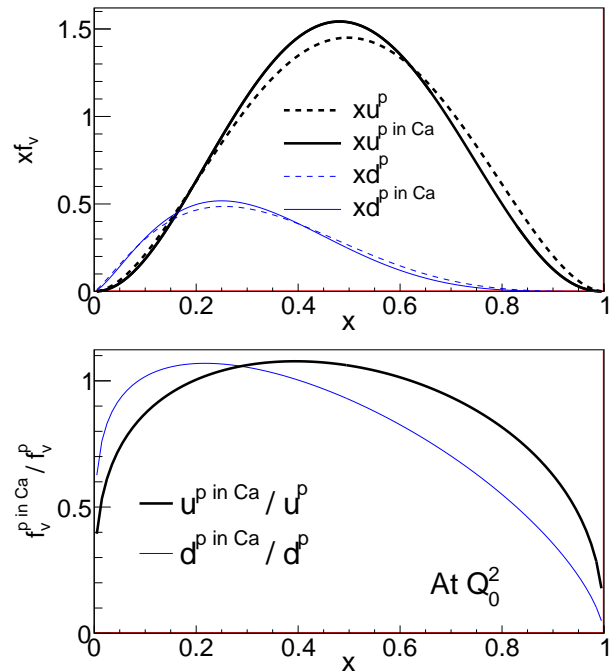


FIG. 1. The valence quark distributions of free proton and the bound proton in  $^{40}\text{Ca}$  at  $Q_0^2 = 0.067 \text{ GeV}^2$  are shown in the top panel. The EMC effect from only the nucleon swelling is shown in the bottom panel.

### III. NIMPARTON NUCLEAR PARTON DISTRIBUTION FUNCTIONS

In IMParton global analysis, a nonperturbative input of only three valence quarks is realized for free proton PDFs using DGLAP evolution with parton-parton recombinations [65, 66]. Based on the IMParton analysis, the nIMParton analysis presents a global fit of nuclear PDFs with the nucleon swelling assumption [20, 21]. Different from the traditional nuclear PDF analyses which use some arbitrary functions to model the nuclear effect (the parton distribution ratios) with many parameters, the nIMParton global fit is a model-dependent analysis with the nonperturbative input consisting of only valence quarks, in order to better constrain the nuclear gluon distributions. The nuclear gluon distributions are completely dynamically generated in the DGLAP evolution

with parton-parton recombinations, which are of small bias theoretically.

Using much fewer parameters in the nIMParton analysis, the nucleon swelling factor  $\delta_A$  in Eq. (2) is modeled to be proportional to the Residual Strong Interaction Energy (RSIE), as  $\delta_A = \alpha \times RSIE/A$ .  $\alpha$  is a free parameter and fixed by the global fit.  $RSIE$  is simply the binding energy of strong interaction, defined as the nuclear binding with the Coulomb part subtracted, of the formula  $RSIE = B - B^{\text{Coul.}}$  [67]. The nuclear binding  $B$  is taken from the experimental measurement, and  $B^{\text{Coul.}}$  is calculated with  $-a_c Z(Z-1)A^{-1/3}$  ( $a_c = 0.71$  MeV). The  $RSIE$  with different  $A$ ,  $Z$  and  $N$  can easily be calculated. For nIMParton, the  $A$ ,  $Z$ , and  $N$  dependence of the EMC effect are interpreted as the dependence on the binding energy of residual strong force (the  $RSIE$ ). The EMC effect of unmeasured nuclei also can be predicted, using  $\alpha = 0.00563$  MeV $^{-1}$  determined with nIMParton global fit. The nuclear PDFs at high  $Q^2$  are calculated using DGLAP equations with the modified nuclear valence distributions at  $Q_0^2$ . The  $Q^2$ -dependence of the EMC effect is weak at high  $Q^2$ , which is illustrated in Fig. 2.

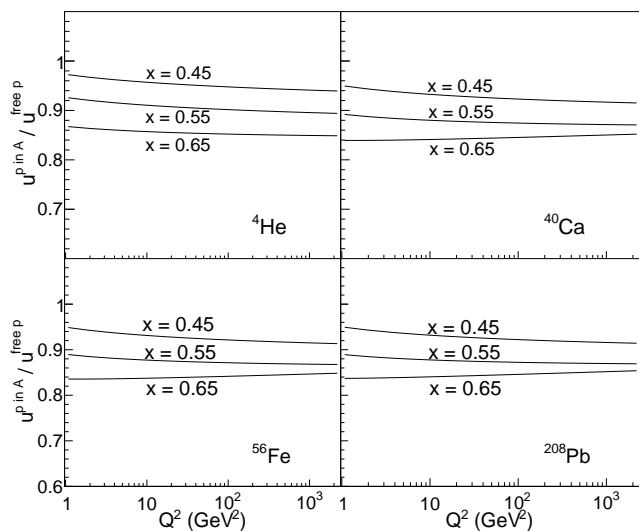


FIG. 2. The  $Q^2$ -dependence of the nuclear effect for  ${}^4\text{He}$ ,  ${}^{40}\text{Ca}$ ,  ${}^{56}\text{Fe}$  and  ${}^{208}\text{Pb}$ .

In addition to the nucleon swelling modeling above, a convolution formula and the parton-parton recombination effect are taken to describe the Fermi motion effect at large  $x$  and the nuclear shadowing at small  $x$ , respectively. No direct effects of virtual mean-field mesons are taken to calculate the nuclear quark distributions in nIMParton analysis [20].

In short, nIMParton is a model-dependent global fit of nuclear DIS data. In the model, the EMC effect exhibit some difference between up valence quark and down valence quark, which is due to the shape difference between up valence distribution and down valence distribution. There are no sea quarks and no gluons in the

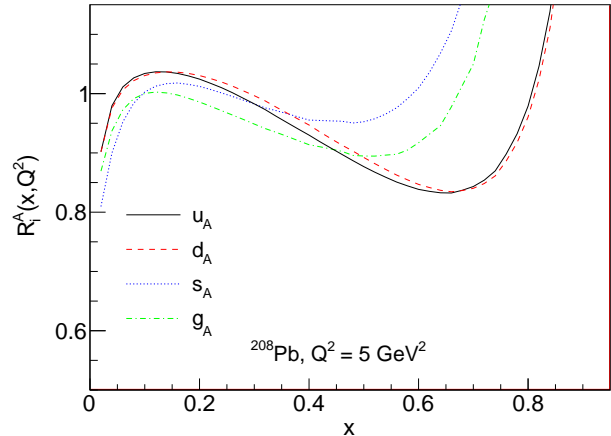


FIG. 3. Nuclear modification factors of different flavors from nIMParton [20, 21] are shown.  $R_i^A$  here is defined as  $Af_i^A/[Zf_i^p + Nf_i^n]$ , in which  $f_i^A$  is calculated with Eq. (3).

nonperturbative input at the initial scale  $Q_0^2$  [20]. All sea quarks and gluons are dynamically generated from the radiations of valence quarks in the DGLAP evolution. Hence, it is not surprising that the EMC effect of strange quark is different from valence quarks. In experiments, the nuclear PDFs are the average distributions of all bound nucleons. The nuclear PDF of flavor  $i$  can be calculated from the nIMParton nuclear modification factors with the following formula,

$$f_i^A(x, Q^2) = \left[ ZR_i^{\text{bound } p}(x, Q^2)f_i^p(x, Q^2) + (A - Z)R_i^{\text{bound } n}(x, Q^2)f_i^n(x, Q^2) \right] / A, \quad (3)$$

where  $Z$ ,  $A$ ,  $f_i^A(x, Q^2)$ ,  $f_i^p$  and  $f_i^n$  are atomic number, mass number, nuclear PDF, proton PDF and neutron PDF respectively. The nuclear modifications  $R_i^{\text{bound } p}(x, Q^2)$  and  $R_i^{\text{bound } n}(x, Q^2)$  can be accessed from the web [21]. For the calculations in this paper, the isospin symmetry is assumed between proton and neutron, which implies  $f_u^n = f_d^p$ ,  $f_d^n = f_u^p$ ,  $f_{\bar{u}}^n = f_{\bar{d}}^p$  and  $f_{\bar{d}}^n = f_{\bar{u}}^p$ .

The results for the nuclear modification factors of Eq. (3) are shown in Fig. 3. The differences among the ratios indicate the flavor-dependence of the nuclear medium effect. Under the nIMParton data set, the differences are large among the ratios of valence quark distribution, sea quark distribution, and gluon distribution while the nuclear modification difference is small for up quark distribution and down quark distribution in a nucleus, showing the maximum around  $x = 0.5$ . In the anti-shadowing region the sea quarks are slightly suppressed, which is consistent with the Drell-Yan data from E772 [68] and E866 [69]. These experiments measured the DY di-muon production in the range of  $0.01 < x < 0.3$  for Carbon, Calcium, Iron and Tungsten nuclei, and found no enhancements of the nuclear anti-quark distributions.

#### IV. PARITY-VIOLATING DEEP INELASTIC SCATTERING

By using the polarized electron probe, the parity-violating DIS experiment under high luminosity would present an important test on the difference between the EMC effect of up quark and that of down quark [14]. This idea to check the flavor-dependent modifications of nuclear medium is to measure the difference between the traditional  $F_2$  ratio and the  $\gamma Z$  interference structure function ratio. The ratio definitions of the EMC effect for both the traditional DIS and the  $\gamma Z$  interference structure functions are written as,

$$R^i = \frac{F_{2A}^i}{F_{2A}^{i,naive}} = \frac{F_{2A}^i}{ZF_{2p}^i + NF_{2n}^i}, \quad (i = \gamma, \gamma Z) \quad (4)$$

where  $F_{2A}^\gamma$  and  $F_{2A}^{\gamma Z}$  are the traditional unpolarized structure function and the  $\gamma Z$  interference structure function respectively. The dominant term of the cross-section asymmetry between the positive and the negative electron helicity is denoted as  $a_2$  [14], which is directly connected to the ratio of  $F_{2A}^\gamma$  and  $F_{2A}^{\gamma Z}$ . Therefore the  $F_{2A}^{\gamma Z}$  can be extracted combining the  $a_2$  measurement of PVDIS and the traditional  $F_{2A}$  data.

Fig. 4 shows the  $a_2$  of Lead using only up and down quark distributions with the application of nIMParton nuclear modification factors. The calculations of  $a_2$  are given with the formula in Ref. [14], which assumes  $s + \bar{s} \ll u + d + \bar{u} + \bar{d}$ . One can find that the  $a_2$  value actually depends on the PDF set used. Nevertheless, both PDF sets show small changes of  $a_2$  curves using nIMParton nuclear modifications, which is different from the prediction of CBT model. There is an obvious difference between the naive  $a_2$  and the  $a_2$  with CBT nuclear correction [14]. Moreover, the  $x$ -dependence of  $a_2$  of  $^{208}\text{Pb}$  predicted from CBT model and that from nIMParton nuclear PDFs show clearly different behaviors. The  $a_2$  curve applying nIMParton nuclear PDFs is rather flat, while the  $a_2$  curve goes up quickly with  $x$  approaching one in the CBT model (see Fig. 1 in Ref. [14]). Fig. 5 shows  $a_2$  of Lead with strange quark distribution included. Adding strange quark distribution changes much  $a_2$  in small  $x$  region only. Therefore the  $a_2$  measurement in the valence region is feasible to distinguish the different models about the flavor-dependent EMC effect.

Fig. 6 shows the comparisons between the traditional structure function ratio and the  $\gamma Z$  interference structure function ratio. The formula to calculate these structure functions in terms of up and down quark distributions can be found in Ref. [14]. Based on nIMParton nuclear modifications, the difference between  $R_{Lead}^\gamma$  and  $R_{Lead}^{\gamma Z}$  is trivial. This conclusion is clearly different from that predicted by CBT model. The CBT model predicts a noticeable difference between  $R_{Lead}^\gamma$  and  $R_{Lead}^{\gamma Z}$  based on the flavor-dependent nuclear force (the  $\rho_0$  mean field). The data points in Fig. 6 show the extrapolated EMC ratios for infinite nuclear matter [70]. The heavy nu-

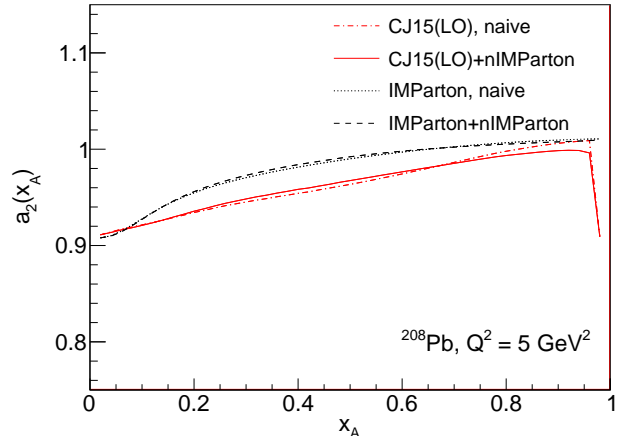


FIG. 4. The  $a_2$  term of the analyzing power of longitudinally polarized electron DIS scattering on  $^{208}\text{Pb}$  target. In the calculations, the strange quark distribution and the heavy quark distributions are neglected. CJ15(LO) PDF is taken from Refs. [71, 72]. IMParton PDF is taken from Refs. [65, 66]. nIMParton nuclear correction factor is from Refs. [20, 21].

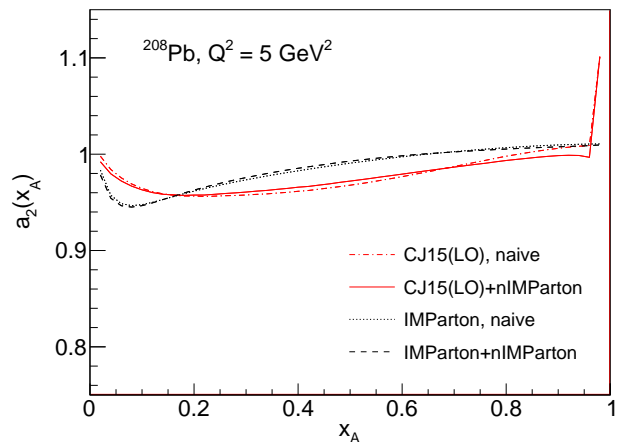


FIG. 5. The  $a_2$  term of the analyzing power of longitudinally polarized electron DIS scattering on  $^{208}\text{Pb}$  target. Up, down, and strange quark distributions are all used in the calculations. CJ15(LO) PDF is taken from Refs. [71, 72]. IMParton PDF is taken from Refs. [65, 66]. nIMParton nuclear correction factor is from Refs. [20, 21].

cleus  $^{208}\text{Pb}$  can be viewed as the infinite nuclear matter approximately. The predictions with nIMParton are consistent with the data. The  $R_{Lead}^{\gamma Z}$  extracted from PVDIS experiment is of significance to check the predictions of the general nucleon swelling effect and of the isovector field effect.

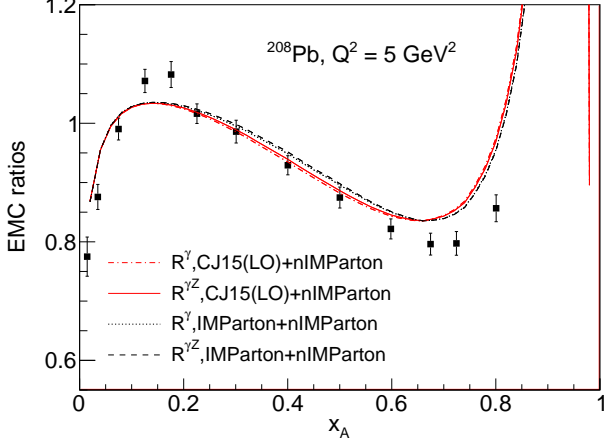


FIG. 6. The traditional DIS and the  $\gamma Z$  interference structure function ratios of  $^{208}\text{Pb}$  to free nucleons. In the calculations, the strange quark distribution and the heavy quark distributions are ignored. CJ15(LO) PDF is taken from Refs. [71, 72]. IMParton PDF is taken from Refs. [65, 66]. nIMParton nuclear correction factor is from Refs. [20, 21]. The square points depict an extrapolation for infinite nuclear matter using a local density approximation [70].

## V. PION-INDUCED DRELL-YAN PROCESS

Pion-induced Drell-Yan process is also a sensitive experimental tool to probe the flavor-dependent EMC effect [15]. The DY cross section ratios which are sensitive to the nuclear up and down quark distributions are denoted as,

$$\begin{aligned} R_{\pm}^{DY} &= \frac{\sigma^{DY}(\pi^+ + A)}{\sigma^{DY}(\pi^- + A)} \approx \frac{d_A(x)}{4u_A(x)} \\ R_{-}^{DY,A/D} &= \frac{\sigma^{DY}(\pi^- + A)}{\sigma^{DY}(\pi^- + D)} \approx \frac{u_A(x)}{u_D(x)} \\ R_{-}^{DY,A/H} &= \frac{\sigma^{DY}(\pi^- + A)}{\sigma^{DY}(\pi^- + H)} \approx \frac{u_A(x)}{u_p(x)} \end{aligned} \quad (5)$$

where A, D, and H represent the nuclear, the deuteron and the hydrogen targets respectively.  $R_{\pm}$  measures the nuclear down quark to up quark ratio, while  $R_{-}$  measures the nuclear medium modification of up quark distribution. The precise data of these DY cross-section ratios would provide some stringent constraints to various models on the EMC effect.

The comparisons between the predictions from nIMParton nuclear modifications and the existing pionic DY data are shown in Fig. 7. The upper panels indicate that the nIMParton model describe well the EMC effect of up quark distribution for both Tungsten and Platinum targets. From the lower panels, we find that the nIMParton nuclear modifications may not describe well the nuclear down quark to up quark ratios. However the uncertainties of the  $R_{\pm}$  data are quite big up to date. The CBT model successfully interpret well all the data except the

NA10 data (see Fig. 2 in Ref. [15]). We need the possible future pion-induced Drell-Yan experiments to test the predictions and to quantify the flavor-dependence of the EMC effect.

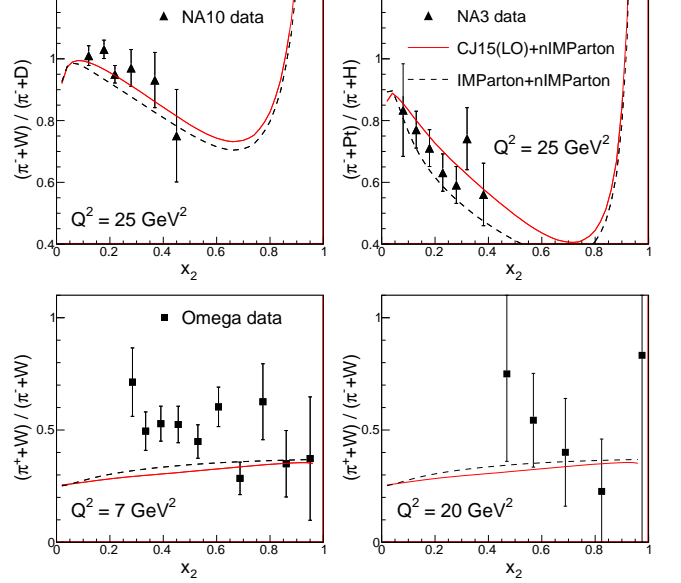


FIG. 7. The ratios between the cross-sections of different pion-induced Drell-Yan processes. CJ15(LO) PDF is taken from Refs. [71, 72]. IMParton PDF is taken from Refs. [65, 66]. nIMParton nuclear correction factor is from Refs. [20, 21]. The triangles represent the NA10 [73] and NA3 [74] data. The squares represent the Omega data [75].

## VI. W-BOSON PRODUCTION IN PROTON-NUCLEUS COLLISIONS

Chang et al. suggest that it is another possible method to explore the flavor-dependent EMC effect by measuring the differential cross-sections of W-boson production in proton-nucleus collisions [16]. The experimental observables related to the topic are the cross-section ratios which are defined as the followings:

$$\begin{aligned} R_{A/D}^{+}(x_F) &= \frac{\frac{d\sigma}{dx_F}(p + A \rightarrow W^{+} + X)}{\frac{d\sigma}{dx_F}(p + D \rightarrow W^{+} + X)} \approx \frac{u_A(x_2)}{u_D(x_2)}, \\ R_{A/D}^{-}(x_F) &= \frac{\frac{d\sigma}{dx_F}(p + A \rightarrow W^{-} + X)}{\frac{d\sigma}{dx_F}(p + D \rightarrow W^{-} + X)} \approx \frac{d_A(x_2)}{d_D(x_2)}, \\ R_{A/D}^{\pm}(x_F) &= \frac{\frac{d\sigma}{dx_F}(p + A \rightarrow W^{+} + X)}{\frac{d\sigma}{dx_F}(p + A \rightarrow W^{-} + X)} \approx \frac{\bar{d}_p(x_1)u_A(x_2)}{\bar{u}_p(x_1)d_A(x_2)}, \end{aligned} \quad (6)$$

in which  $x_F = x_1 - x_2$  is the Feynman  $x$  variable of the W-boson,  $x_1$  and  $x_2$  are the momentum fractions carried by the partons in the initial proton and in the initial nucleus respectively. A and D denote the heavy nucleus and the deuteron respectively.

Fig. 8 shows the predictions of the cross-section ratios of W-boson production in different models for the proton-Lead collisions. The  $Q$  scale in the parton model calculations is chosen to be the W-boson mass scale. It is interesting to find that the result based on nIMParton nuclear corrections is between that of CBT model and that of CBT model without the isovector meson force. These different model predictions can be verified with the apparatuses at LHC or RHIC in the runs of high energy proton-nucleus collisions under high luminosities.

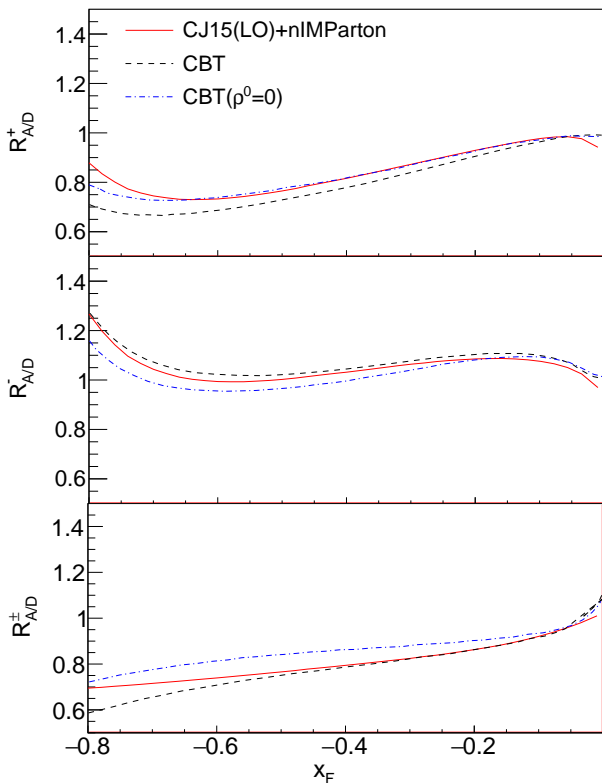


FIG. 8. nIMParton predictions of the cross-section ratios of W-boson productions in proton-nucleus collisions (between  $^{208}\text{Pb}$  and deuteron, see text for explanations) with the center-of-mass energy of  $\sqrt{s} = 5.520$  TeV, compared with the CBT model [17–19]. CJ15(LO) PDF is taken from Refs. [71, 72]. nIMParton nuclear correction factor is from Refs. [20, 21].

## VII. SPECTATOR-TAGGED DEEP INELASTIC SCATTERING

Spectator-tagged DIS from deuterium and  $^4\text{He}$  are proposed to be measured using CLAS12 detectors combined with the ALERT detector specialized in detecting the low energy spectator nuclei [24]. By tagging the nuclear recoil spectators ( $^4\text{He}(e, e' ^3\text{H})X$  and  $^4\text{He}(e, e' ^3\text{He})X$ ), we can probe the nuclear effect difference between the bound proton and the bound neutron. The data of medium

modified nucleons would provide some novel and important tests on many models describing the EMC effect.

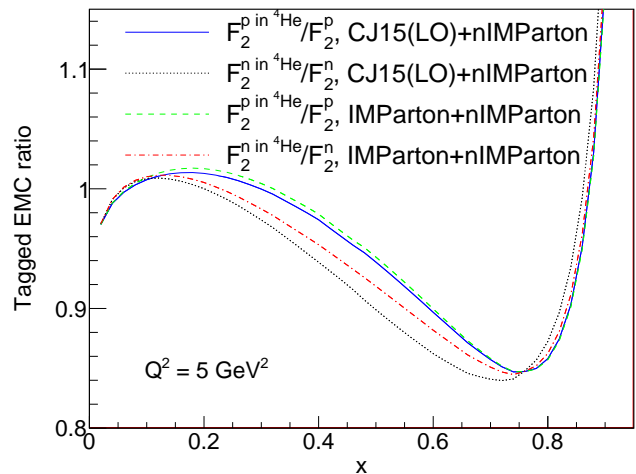


FIG. 9. Predictions of the spectator-tagged EMC ratios for  $^4\text{He}$  nucleus. The PDFs of free proton and free neutron are taken from CJ15 [71, 72] and IMParton [65, 66]. The nuclear modifications of PDFs in bound nucleons are adopted from nIMParton global analysis [20, 21].

Measurement in DIS region displays the structure functions of nucleons. In the leading order and ignoring the contributions of heavy quarks, the proton structure function is expressed as  $F_2^p = x(\frac{4}{9}u^p + \frac{1}{9}d^p + \frac{1}{9}s^p)$ . Under the assumption of isospin symmetry, the neutron structure function is expressed as  $F_2^n = x(\frac{4}{9}u^n + \frac{1}{9}d^n + \frac{1}{9}s^n) = x(\frac{4}{9}d^p + \frac{1}{9}u^p + \frac{1}{9}s^p)$ . It is easy to see that the flavor-dependence of the nuclear modifications on quark distributions could result in the difference of the EMC effect between medium modified proton and medium modified neutron. If the nuclear modifications on up and down quarks are the same, then the EMC ratios for bound proton and bound neutron are identical (ignoring the contribution of strange quark in the large  $x$  region).

Fig. 9 shows the EMC effects of bound proton and bound neutron inside the  $^4\text{He}$  nucleus. In the calculations, the nuclear modifications on parton distributions are taken from nIMParton analysis [20, 21]. The EMC ratios for bound proton and for bound neutron exhibit some differences, especially around  $x = 0.5$ . Therefore, the tagged-DIS experiment has the potential to test nIMParton predictions and the nucleon swelling model used to soften the valence quark distributions. To quantify the EMC effect of the bound neutron, the free neutron structure function data is needed as the denominator. Fortunately, the state-of-the-art measurement of the nearly free neutron structure function is currently realized by the BoNUS Collaboration at JLab [76–78].

To clearly demonstrate the magnitude difference of the EMC effect between the bound proton and the bound neutron, the ratio of the nuclear EMC effect is shown in Fig. 10. It is shown that at  $x$  around 0.5, the difference between the EMC ratios of the bound proton and bound

neutron is at the maximum of about 3% relatively. The ALERT experiment will be able to explore the variation of the nuclear modification within the statistical error bars of 1 to 2% [24]. Hence, the ALERT detector with CLAS12 would play an important role in unveiling the issue on the isospin-dependent nuclear medium effect.

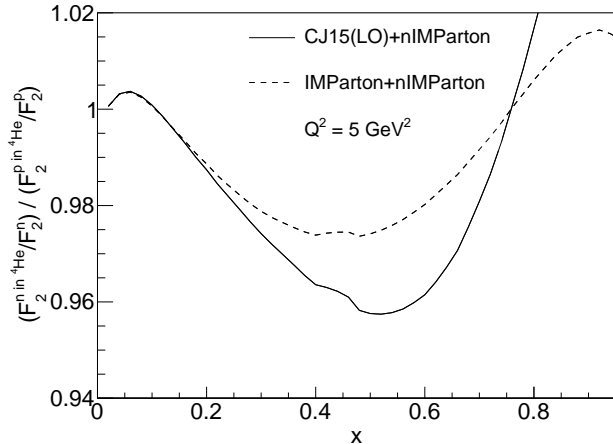


FIG. 10. The ratio of the nuclear modification factor on neutron  $F_2$  to the nuclear modification factor on proton  $F_2$ , for  ${}^4\text{He}$  nucleus. The PDFs of free proton and free neutron are taken from CJ15 [71, 72] and IMParton [65, 66] for the calculations. The nuclear modifications of PDFs in bound nucleons are adopted from nIMParton global analysis [20, 21].

## VIII. SUMMARY

We discussed the new aspect of the EMC effect, the flavor-dependence, using nIMParton nuclear modification factors. The forms of valence quark distributions are modified according to the Heisenberg uncertainty principle [20]. The nIMParton global analysis assumes the same enlargement of the confinement size for both proton and neutron, and for both up valence quark and down valence quark. Therefore, the isospin-dependence of the EMC effect in the model is due to the fact that the down valence quark distribution is narrower and softer than up valence quark distribution. The CBT model with the isospin-dependent nuclear forces predicts larger nuclear effect difference between up and down quark distributions than that of nIMParton, for heavy nuclei with  $N \neq Z$ .

The flavor-dependent EMC effect based on nIMParton nuclear PDFs is demonstrated with the predictions of various observables in the suggested experiments of PVDIS, pion-induced Drell-Yan, W-boson production in p-A collisions, and the tagged-DIS processes. The nIMParton predictions are consistent with the Drell-Yan data decades ago. However we need more experiments in the future to explicitly differentiate various models on EMC effect. The experiment on CLAS12 with the ALERT detector at JLab is available to test the models on the flavor dependence of the nuclear effect in large  $x$  region, which could provide a timely and critical insight of the new aspect of the EMC effect.

One aim of the ALERT experiment is to measure the nuclear effect of the mean-field nucleon and of the short-range correlated nucleon [24]. With the technique of tagging the recoil nuclei, the EMC effect as a function of nucleon off-shellness can be deduced. In this work, the EMC effect investigated is the average EMC effect of the nucleons of different virtualities. If the confinement enlargement goes up as the local density increase, the EMC effect should consequently enhanced for the case of high momentum nuclear spectator recoil.

- 
- [1] J. J. Aubert et al. (The European Muon Collaboration), Phys. Lett. B **123**, 275 (1983).
  - [2] M. Arneodo, Phys. Rept. **240**, 301 (1994).
  - [3] D. Geesaman, K. Saito, and A. W. Thomas, Annu. Rev. Nucl. Part. Sci. **45**, 337 (1995).
  - [4] P. R. Norton, Rep. Prog. Phys. **66**, 1253 (2003).
  - [5] J. Arrington, A. Daniel, D. B. Day, N. Fomin, D. Gaskell, and P. Solvignon, Phys. Rev. C **86**, 065204 (2012).
  - [6] Or Hen, Gerald A. Miller, Eli Piassetzky, and Lawrence B. Weinstein, Rev. Mod. Phys. **89**, 045002 (2017).
  - [7] S. Malace, D. Gaskell, D. W. Higinbotham, and I. C. Cloët, Int. J. Mod. Phys. E **23**, 1430013 (2014).
  - [8] R. P. Bickerstaff and G. A. Miller, Phys. Rev. D **34**, 2890 (1986).
  - [9] K. J. Eskola, V. J. Kolhinen, and P. V. Ruuskanen, Nucl. Phys. B **535**, 351 (1998).
  - [10] K. J. Eskola, V. J. Kolhinen, and C. A. Salgado, Eur. Phys. J. C **9**, 61 (1999).
  - [11] J. Seely et al., Phys. Rev. Lett. **103**, 202301 (2009).
  - [12] L. B. Weinstein, E. Piassetzky, D. W. Higinbotham, J. Gomez, O. Hen, and R. Shneor, Phys. Rev. Lett. **106**, 052301 (2011).
  - [13] O. Hen, E. Piassetzky, and L. B. Weinstein, Phys. Rev. C **85**, 047301 (2012).
  - [14] I. C. Cloët, W. Bentz, and A. W. Thomas, Phys. Rev. Lett. **109**, 182301 (2012).
  - [15] D. Dutta, J. C. Peng, I. C. Cloët, and D. Gaskell, Phys. Rev. C **83**, 042201 (2011).
  - [16] W. C. Chang, I. C. Cloët, D. Dutta, J. C. Peng, Phys. Lett. B **720**, 188 (2013).
  - [17] I. C. Cloët, W. Bentz, and A. W. Thomas, Phys. Lett. B **642**, 210 (2006).
  - [18] I. C. Cloët, W. Bentz, and A. W. Thomas, Phys. Rev. Lett. **102**, 252301 (2009).



- [19] W. Bentz, I. C. Cloët, J. T. Londergan, and A. W. Thomas, *Phys. Lett. B* **693**, 462 (2010).
- [20] Rong Wang, Xurong Chen, and Qiang Fu, *Nucl. Phys. B* **920**, 1 (2017).
- [21] <https://github.com/lukeronger/nIMParton>
- [22] W. R. Armstrong, J. Arrington. I. Cloët et al., arXiv:1708.00835.
- [23] W. R. Armstrong, J. Arrington. I. Cloët et al., arXiv:1708.00888.
- [24] W. R. Armstrong, J. Arrington. I. Cloët et al., arXiv:1708.00891.
- [25] C. A. García Canal, E. M. Santangelo, and H. Vucetich, *Phys. Rev. Lett.* **53**, 1430 (1984).
- [26] M. Staszel, J. Rożynek, and G. Wilk, *Phys. Rev. D* **29**, 2638 (1984).
- [27] S. V. Akulinichev, S. Shlomo, S. A. Kulagin, and G. M. Vagradov, *Phys. Rev. Lett.* **55**, 2239 (1985).
- [28] L. L. Frankfurt, M. I. Strikman, *Phys. Lett. B* **183**, 254 (1987).
- [29] Hong Jung and Gerald A. Miller, *Phys. Lett. B* **200**, 351 (1988).
- [30] C. Ciofi degli Atti, L. Kaptari, and S. Scopetta, *Euro. Phys. J. A* **5**, 191 (1999).
- [31] G. V. Dunne and A. W. Thomas, *Phys. Rev. D* **33**, 2061 (1986).
- [32] F. Gross and S. Liuti, *Phys. Rev. C* **45**, 1374 (1992).
- [33] S. A. Kulagin, G. Piller, and W. Weise, *Phys. Rev. C* **50**, 1154 (1994).
- [34] S. A. Kulagin and R. Petti, *Nucl. Phys. A* **765**, 126 (2006).
- [35] S. A. Kulagin and R. Petti, *Phys. Rev. C* **90**, 045204 (2014).
- [36] F. E. Close, R. G. Roberts, and G. G. Ross, *Phys. Lett. B* **129**, 346 (1983).
- [37] R. L. Jaffe, F. E. Close, R. G. Roberts, and G. G. Ross, *Phys. Lett. B* **134**, 449 (1984).
- [38] O. Nachtmann and H. J. Pirner, *Z. Phys. C* **21**, 277 (1984).
- [39] F. E. Close, R. L. Jaffe, R. G. Roberts, and G. G. Ross, *Phys. Rev. D* **31**, 1004 (1985).
- [40] F. E. Close, R. G. Roberts, and G. G. Ross, *Nucl. Phys. B* **296**, 582 (1988).
- [41] R. L. Jaffe, *Phys. Rev. Lett.* **50**, 228 (1983).
- [42] C. E. Carlson and T. J. Havens, *Phys. Rev. Lett.* **51**, 261 (1983).
- [43] M. Chemtob and R. Peschanski, *J. Phys. G* **10**, 599 (1984).
- [44] Gerald A. Miller, *Phys. Rev. Lett.* **53**, 2008 (1984).
- [45] B. C. Clark, S. Hama, B. Mulligan, and K. Tanaka, *Phys. Rev. D* **31**, 617 (1985).
- [46] P. A. M. Guichon, *Phys. Lett. B* **200**, 235 (1988).
- [47] Pierre A. M. Guichon, Koichi Saito, Evgenii Rodionov, and Anthony W. Thomas, *Nucl. Phys. A* **601**, 349 (1996).
- [48] K. Saito, K. Tsushima, and A. W. Thomas, *Prog. Part. Nucl. Phys.* **58**, 1 (2007).
- [49] Ingo Sick, *Phys. Lett. B* **157**, 13 (1985).
- [50] P. B. Siegel, W. B. Kaufmann, and W. R. Gibbs, *Phys. Rev. C* **31**, 2184 (1985).
- [51] G. E. Brown, C. B. Dover, P. B. Siegel, and W. Weise, *Phys. Rev. Lett.* **60**, 2723 (1988).
- [52] Y. Mardor et al., *Phys. Rev. Lett.* **65**, 2110 (1990).
- [53] N. N. Nikolaev, *Z. Phys. C* **32**, 537 (1986).
- [54] Makoto Oka and R. D. Amado, *Phys. Rev. C* **35**, 1586 (1987).
- [55] G. Kälbermann, L. L. Frankfurt, and J. M. Eisenberg, *Phys. Lett. B* **329**, 164 (1994).
- [56] J. Dukelsky, F. Fernández, and E. Moya de Guerra, *J. Phys. G* **21**, 317 (1995).
- [57] Jason R. Smith and Gerald A. Miller, *Phys. Rev. Lett.* **91**, 212301 (2003).
- [58] Jishnu Dey and Mira Dey, *Phys. Lett. B* **176**, 469 (1986).
- [59] V. Barone, M. Genovese, N. N. Nikolaev, E. Predazzi, and B. G. Zakharov, *Z. Phys. C* **58**, 541 (1993).
- [60] L. L. Frankfurt and M. I. Strikman, *Nucl. Phys. B* **250**, 143 (1985).
- [61] Yunhua Zhang, Lijing Shao, and Bo-Qiang Ma, *Nucl. Phys. A* **828**, 390 (2009).
- [62] Arifuzzaman, Pervez Hoodbhoy, and Sajjad Mahmood, *Nucl. Phys. A* **480**, 469 (1988).
- [63] Chr. V. Christov, E. Ruiz Arriola, and K. Goeke, *Nucl. Phys. A* **510**, 689 (1990).
- [64] J. V. Noble, *Phys. Lett. B* **178**, 285 (1986).
- [65] Rong Wang and Xu-Rong Chen, *Chinese Physics C* **41**, 053103 (2017).
- [66] <https://github.com/lukeronger/IMPparton>
- [67] Rong Wang and Xurong Chen, *Phys. Lett. B* **743**, 267 (2015).
- [68] D. M. Alde et al., *Phys. Rev. Lett.* **64**, 2479 (1990).
- [69] M. A. Vasiliev et al. (FNAL E866/NuSea Collaboration), *Phys. Rev. Lett.* **83**, 2304 (1999).
- [70] Ingo Sick and Donal Day, *Phys. Lett. B* **274**, 16 (1992).
- [71] A. Accardi, L. T. Brady, W. Melnitchouk, J. F. Owens, and N. Sato, *Phys. Rev. D* **93**, 114017 (2016).
- [72] <https://www.jlab.org/theory/cj/>
- [73] P. Bordalo et al. (NA10 Collaboration), *Phys. Lett. B* **193**, 368 (1987).
- [74] J. Badier et al. (NA3 Collaboration), *Phys. Lett. B* **104**, 335 (1981).
- [75] M. Corden et al., *Phys. Lett. B* **96**, 417 (1980).
- [76] N. Baillie et al. (CLAS Collaboration), *Phys. Rev. Lett.* **108**, 142001 (2012).
- [77] N. Baillie et al. (CLAS Collaboration), *Phys. Rev. Lett.* **108**, 199902 (2012).
- [78] S. Tkachenko et al. (CLAS Collaboration), *Phys. Rev. C* **89**, 045206 (2014).